High temperature translaminar fracture of woven-ply thermoplastic laminates in tension and in compression

Juan Daniel Pujols Gonzalez, Benoît Vieille, Christophe Bouvet

High temperature translaminar fracture of woven-ply thermoplastic laminates in tension and in compression

Juan Daniel Pujols Gonzalez [a], Benoit Vieille [a,*], Christophe Bouvet [b]

[a] INSA Rouen Normandie, Groupe de Physique des Matériaux (UMR CNRS 6634), Equipe ERMECA, 76801 St Etienne du Rouvray, France
[b] Université de Toulouse, Institut Clément Ader (UMR CNRS 5312), ISAE-SUPAERO, 10 av. E. Belin – 31055, Toulouse cedex 4, France

Keywords:
Translaminar fracture toughness
Woven-ply laminate
Thermoplastic
High temperature
Digital image correlation
Critical energy release rate

A B S T R A C T

The translaminar fracture behavior of three composite laminates, based on thermoplastic matrix PEEK reinforced by a woven carbon fibers obtained by consolidation process, has been studied by means of Compact Tension (CT) and Compact Compression (CC) tests. An orthotropic laminate and two quasi-isotropic laminates, have been tested at room temperature (RT) and at 150 °C (i.e. for a temperature slightly higher than the glass transition temperature T_g), with the purpose of evaluation the influence of the stacking sequence and the temperature on the damage mechanisms. The CT type tests show that the temperature influence on the overall mechanical response remains low. In contrast, the CC type tests show a decrease in the mechanical resistance and an augmentation in the global ductile behavior. By means of the 2D Digital Image Correlation and the implementation of a algorithm based on the sigma indicator (confidence interval in the area of interest), the crack propagation was measured during loading, then the G-R curves have been obtained from the compliance method. In tension, there is an increase in the translaminar fracture toughness with the laminate thickness and a slight improvement in this one due to the influence of temperature. In compression, the temperature strongly decreases the translaminar fracture toughness.

1. Introduction

The widespread use of organic matrix composites in many industrial sectors has been confronted with the need to understand and quantify the fracture mechanisms within materials whose behaviour is highly heterogeneous and anisotropic. In addition, they can be subjected to different mechanical loads, but also to different environmental conditions (temperature, humidity, etc.) when it comes to aeronautical applications. Among the main damage modes observed in composite laminates, the breaking of fibers in tension or compression is less studied, compared to delamination. These different damage mechanisms result in the development of a "Fracture Process Zone" (FPZ) in regions where the material is damaged by high stress concentrations, i.e. near holes, notches, or manufacturing defects [1,2]. Depending on the nature of the constituent materials, and the stacking sequence, laminated composites are generally characterized by three primary failure modes (Fig. 1): interlaminar, intralaminar and translaminar failure. These modes are observed at different scales: microscopic scale (fiber/resin interaction), mesoscopic scale (laminate ply) and macroscopic scale (laminate). Translaminar fracture occurs at the mesoscopic scale, with the breakage of fiber bundles. There are two modes of translaminar failure in fiber-reinforced laminates: fiber breakage in tension and in compression [3,4]. In the case of compressive loadings, fiber failure is

* Corresponding author.
E-mail address: benoit.vieille@insa-rouen.fr (B. Vieille).

https://doi.org/10.1016/j.engfracmech.2021.107616

Nomenclature

4PB	Four Points Bend specimen
5HS	five-harness satin weave
a	crack length
a_0	initial value of crack length
C	specimen load-line compliance
C_I	orthotropic elastic coefficient in plane-stress conditions
C7/PEEK	seven carbon-PEEK 5HS woven plies quasi-isotropic laminate
C8/PEEK	eight carbon-PEEK 5HS woven plies orthotropic laminate
CC	Compact Compression specimen
CG/PEEK	fourteen carbon-PEEK 5HS woven plies with two outer glass-PEEK woven plies quasi-isotropic laminate
CT	Compact Tension specimen
d	displacement applied
DIC	Digital Image Correlation
E_x	Young's modulus in$x$
E_y	Young's modulus in$y$
ESET	Eccentrically loaded Single-Edge-notch Tensile
$f(a/w)$	geometric correction function for a specimen of finite width
F_T	Fracture Tensile/Compression function
FPZ	Fracture Process Zone
$G_{I_c}^{lam}$	critical energy release rate of the laminate
$G_I^C\|_{compression}$	strain energy release rate in compression
$G_I^C\|_{tension}$	strain energy release rate in tension
G_{xy}	shear modulus
G-R	G-based crack extension resistance
K_{I_c}	critical stress intensity factor in mode I
P	load
P_c	critical load
PEEK	PolyEther Ether Ketone
PMC	Polymer Matrix Composites
RT	room temperature
SENB	Single Edge Notched Bending specimen
SENT	Single Edge Notched Tension specimen
t	specimen thickness
T_g	glass transition temperature
TP	thermoplastic
VCCT	Virtual Crack Closure Technique
w	specimen width
ε_{xy}	shear deformation
ν_{xy}	Poisson's ratio
Δa	crack length

mainly due to the formation of fiber buckling bands (also known as kink-bands). Fracture toughness plays a fundamental role in the damage tolerance of a composite structure. It depends on the stacking sequence of the laminate [6,10–11,20], the loading conditions and the architecture of the reinforcement. Most of the studies dealing with translaminar mode I (opening) failure of multidirectional laminates are based on the quantification of the fracture toughness of unidirectional-ply laminates [3,5–14], while very few studies are dealing with woven-ply laminates [4,15–19].

1.1. Experimental estimation of translaminar fracture toughness

The ASTM-E1922 standard provides recommendations on specimen geometry for estimating the translaminar fracture toughness of composite materials (Eccentrically loaded Single-Edge-notch Tensile), the use of standards derived from metallic materials is widely used for composite materials [13,21]. Damage growth is characterized by the resistance curve (R-curve), which represents the evolution of the critical strain energy release rate as a function of the macroscopic crack length. There are different specimens geometries to induce stable crack growth and to measure the translaminar fracture toughness: Compact Tension (CT) and Compact Compression (CC) [3–6,8,10–11,14,16–17,19–20], three-/four-point bending [7,9,12,15,19] and "Eccentrically loaded Single-Edge-notch Tensile" (ESET) [18,22–23].

CT specimens were mainly used to estimate the translaminar fracture toughness, due to the containment of damage around the crack tip due to fiber failure induced by this type of geometry. Similarly, the measurement of the compressive fracture toughness related to the formation of a buckling band of fibers in compression has been reported in many publications using CC specimens, but the values thus obtained are only valid at the initiation of the fracture and not during propagation, because of the energy dissipated by the delamination that comes along with the propagation of the kink-bands [3,8]. CC specimens are also used to measure compressive fracture toughness related to the formation of a buckling band of fibers in compression In CT specimens there are no significant out-of-plane displacements and the crack propagation data is valid, except only for C8/PEEK orthotropic laminates for which the out-of-plane displacements are observed at testing temperature slightly higher than the glass transition temperature. This may result from its low shear modulus that is obviously much degraded with the temperature [29], and only in this case an anti-buckling device must be used [24]. In CC specimens, the crack growth is mainly related to micro-buckling of the plies at 0°. As a result, the data computation is related to the formation of a kink-band.

Many studies have focused on the development of the best technique for quantifying translaminar fracture toughness [5–6,8] in terms of reproducibility and simplicity of results. Laffan et al concluded that the method of compliance calibration based on effective crack length is the most appropriate method, because it does not require optical measurement of crack growth during the test [5]. The parameters used in this method to determine the length of the crack are a function of a stiffness model (force-displacement) and do not depend on the size of the specimen, they are related to the elastic compliance measured from the force-displacement curve. In another study presented by Catalonatti et al., a digital image correlation technique based on the computation of the J-integral around the crack tip was shown to be suitable for capturing the critical energy release rate associated with the breakage of longitudinal fibers [8].

Some studies have also pointed out that fracture toughness is not an absolute value. Indeed, translaminar fracture toughness depends on the thickness of the plies. Other studies have showed that the increase in fracture toughness is related to the large amount of fiber bundles pullout at 0° [6,10–11], the blocking effect provided for the two 0° plies together triples the value of the translaminar fracture toughness while the blocking resulting from the 45° plies has little effect on the translaminar fracture toughness.

1.2. Translaminar fracture in woven-ply thermoplastic laminates

Over the past fifty years, several studies have been conducted to understand and quantify translaminar fracture toughness in organic matrix composites. Most of them have been dedicated to unidirectional (UD) thermosetting laminates, using two main types of laminates: carbon/epoxy [3–11,14] and glass/epoxy [7,14]. Translaminar fracture in woven ply laminates has been little studied compared to UD-ply laminates. Woven-ply laminates allow the processing of parts with complex geometries and have good damage tolerance. As with unidirectional-ply laminates, the various techniques for quantifying toughness have proven to be well applicable to woven-ply laminates. The characterization of translaminar fracture in woven ply laminates focuses mainly on the thermosetting materials carbon/epoxy [4] and glass/epoxy [4,15–18]. Many studies have concluded that in glass/epoxy woven ply laminates, matrix microcracking is the predominant damage phenomenon at the crack tip [16–18]. Even if this phenomenon is present, the quantification of fracture toughness remains reliable in the case of near-brittle fracture. The behaviour of Polymer Matrix Composites (PMC) is also characterized by temperature dependence [15,25–30]. Numerous studies have been carried out on the influence of high temperatures on interlaminar fracture in unidirectional [25] and woven-ply thermoplastic (TP) laminates [25], but little work has been done on translaminar fracture of woven-ply thermoset laminates [4,17–18] and almost no work has been done on woven ply TP laminates [15]. It should be noted that TP matrix composites are known for their excellent damage tolerance. In a work proposed by Vieille et al. [15], the translaminar fracture behaviour of a hybrid woven laminate of reinforced carbon and glass fibers combined with a PEEK matrix was studied. By means of tests carried out on notched specimens in tensile and three-point bending at room temperature and $T > T_g$, it appears that temperature has little influence on the translaminar fracture toughness in mode I. In addition, it seems to foster the intrinsic toughness at the crack tip and the extrinsic toughness at the mechanical loading zones [31], which results in a slight increase of the R-curve. Table 1 summarizes a few translaminar tensile and compressive fracture toughness values available in the

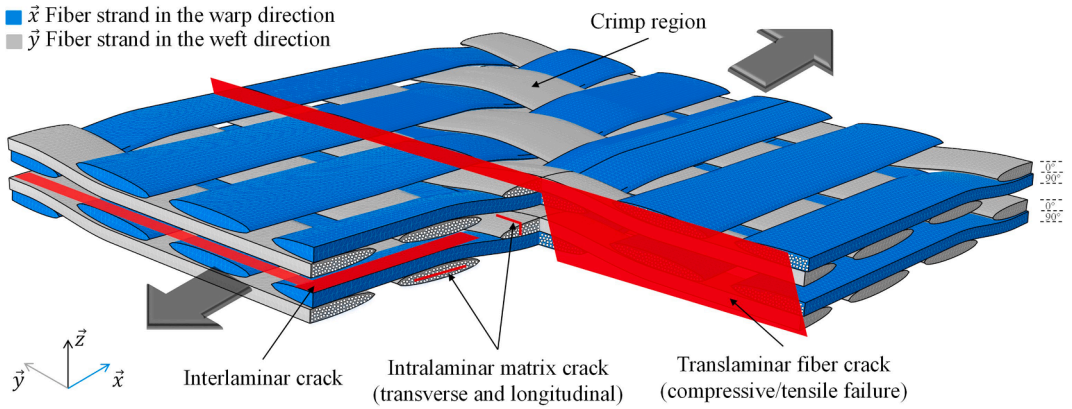

Fig. 1. Overview of ply-level failure modes on a weave pattern.

literature for unidirectional and woven-ply reinforced polymer matrix laminates.

1.3. Objectives of the study

In this context, this study focuses on the experimental characterization of the translaminar fracture of three types of carbon fiber-reinforced thermoplastic laminates. Using CT and CC specimens to induce translaminar fracture in tension and compression, these laminates were tested at room temperature (RT) and at 150 °C when matrix toughness is exacerbated. To our knowledge no translaminar fracture toughness values are available for woven ply PEEK thermoplastic laminates at room temperature and $T > T_g$ [15]. The objective of this study is to analyse the influence of stacking sequence and temperature on the tensile and compressive fracture behaviour of fibers in mode I. This involves measuring the critical energy release rate at initiation and the fracture energy during propagation. Thus, the observation and a post-mortem analysis of damaged areas make it possible to quantify the damage tolerance of TP matrix composites and to understand the influence of temperature on the deformation mechanisms of the TP matrix and ultimately on translaminar fracture.

2. Materials and methods

2.1. Materials

The laminates used in this study are obtained by thermo-compression. They consist of a PEEK thermoplastic matrix reinforced with a continuous carbon fiber fabric (Tenax®-E HTA40 3 K), structured in a 5-harness satin weave (Fig. 1). The average ply thickness of the

Table 1
Summary of experimental data obtained from characterization of the tensile and compressive translaminar failure mode.

Laminate type	Study (year)	Specimen configuration	Polymeric resin Fiber reinforcement	Methods of data reduction	Fracture toughness G_I^C (kJ/m^2)	
					Initiation	Propagation
Unidirectional ply composite laminate	Tension					
	Slepetz et Carlson [14] (1975)	CT	Epoxy Carbon T300/5208	Compliance calibration	21.2	–
	Mahmoud [7] (2003)	SENT	Polyester E-glass	ASTM E399	4.95	–
	Pinho et al. [3] (2006)	CT	Epoxy Carbon T300/913	VCCT and rule of mixtures	91.6	133.0
	Laffan et al. [6] (2010)	CT	Epoxy Carbon T300/920	Modified compliance calibration	57.0	69.0
	Catalonatti et al. [8] (2010)	CT	Epoxy Carbon IM7-8552	Digital Image Correlation	98.7	133.7
	Teixeira et al. [11][a] (2016)	CT	Epoxy Carbon T800s/M21	Modified compliance calibration	46.0–104.0	49.0–160.0
	Compression					
	Pinho et al. [3] (2006)	CC	Epoxy Carbon T300/913	VCCT and rule of mixtures	79.9	–
	Catalonatti et al. [8] (2010)	CC	Epoxy Carbon IM7-8552	Digital Image Correlation	47.5	–
	Laffan et al. [9] (2012)	4 PB	Epoxy Carbon IM7/8552	VCCT	25.9	–
Woven ply composite laminate	Tension					
	Rokbi et al. [17][b] (2011)	CT	Epoxy E-Glass	Compliance calibration	31.9–37.4	42.0–51.0
	Lisle et al. [18][c] (2017)	ESET	Epoxy E-Glass	Infrared thermography	15.8–21.6	61.5–62.5
	Ortega et al. [4] (2017)	CT	Epoxy Hybrid: Carbon G0926/Glass S2	Cohesive law and rule of mixtures	97.0	–
	Vieille at al. [15][d] (2018)	SENB	PEEK Hybrid: Carbon HTA40/E-Glass	ASTM E1820	41.0–44.0	–
	Compression					
	Ortega et al. [4] (2017)	CC	Epoxy Hybrid: Carbon G0926/Glass S2	Cohesive law and rule of mixtures	–	–

[a] Four different 0° ply-block thicknesses ranging from 0.03 mm to 0.12 mm.
[b] Two different fiber directions (warp and weft).
[c] Two different lay-up sequences ($[0°]_2$ and $[\pm 45°]_2$).
[d] Two different temperatures.

laminates is 0.31 mm. Three types of woven laminates are tested (Fig. 2). Two laminates with the same ply ratio at 0°/90° and ± 45°, but with different thicknesses qualified as quasi-isotropic [15,30]:

- [(0/90),(±45),(0/90),(±45),(0/90),(±45),(0/90)] (2.17 mm thick, noted as C7/PEEK)
- $[(0/90)_V,(0/90),(\pm45),(0/90),(\pm45),(0/90),(\pm45),(0/90)]_S$ having two outer plies of glass fabric (5-harness satin weave) and PEEK matrix (4.5 mm thick, noted as CG/PEEK), the 0.08 mm thick $(0/90)_G$ surface glass fabric is used as corrosion protection and electrical protection with the aim of reducing the galvanic torque and thus avoiding galvanic corrosion of aluminum and steel with carbon.
- An eight-ply orthotropic laminate $[(0/90)]_8$ (2.48 mm thick, noted as C8/PEEK).

The main mechanical properties of the elementary ply are specified in Table 2.

2.2. Specimens geometries

The dimensions of the CT and CC specimens were chosen in accordance with ASTM test standard E399-12 [32] (Fig. 3). The specimens are cut from a 600 × 600 mm^2 plate using a water jet machine. The notched area of the CC specimens (Fig. 3b) has been enlarged to avoid contact of the notch faces during compression. The fixing holes of the loading device are machined by means of carbide drills. The ratio between the length of the initial notch and the width of the specimen used is approximately $a/w = 0.45$ for both types of specimens, where a is the crack length and w is the distance from the load line to the right edge of the specimen.

3. Experimental set-up and methods

3.1. Thermo-mechanical testing

All the tests were conducted with a uniaxial servo-hydraulic tension machine MTS 810 equipped with a 100 kN capacity force cell and a thermal chamber. The specimens are held in position by a standardized device in accordance with ASTM-399, which is maintained by the hydraulic grips of the machine and transmits the mechanical load via pins inserted in the holes of the specimens. Six specimens were tested in each configuration (CT and CC) in displacement-controlled mode (1 mm/min) at two temperatures: room temperature (RT) and 150 °C.

3.2. Crack growth measurement by means of a Digital Image Correlation (DIC) technique

A DIC pattern is painted on the specimen surface with a non-periodic texture and without preferred orientation. The use of DIC technique at high temperature requires the use of a high intensity source combined with a fiber optic light guide is used to illuminate the patterns on the surface of the specimen placed into the thermal chamber. A Grasshopper® high-speed monochrome camera allows digital images to be recorded at full resolution (1920 × 1200 pixels), and at a rate of one frames-per-second during thermomechanical loading. The VIC-2D digital image correlation software provides the confidence interval field associated with the convolution factor (sigma indicator) of each pattern in the region of interest [33]. As was defined by Sutton et al., the VIC-2D system utilizes an optimized correlation method to provide full-field two-dimensional displacement and strain [34]. The method compare the digital images for various small regions (known as subsets) throughout the images before and after deformation using fundamental continuum mechanics concepts, locating the positions of each of these subsets after deformation through digital image analysis. When a material discontinuity appears in the pattern, the homogeneous linear mapping in this region does not present deformed surface and the small subset position is not computed.

Using an algorithm implemented in the Scilab code [35], the crack tip is located via the discontinuity of the strain field resulting from the crack propagation (Catalanotti et al. [8] used a similar technique based on the displacement discontinuity within the pattern). A binarization of the full-field strain obtained by the VIC-2D software is applied (Fig. 4). The identification of the damaged and undamaged areas in the region of interest is associated with a F_T function, which takes values of:

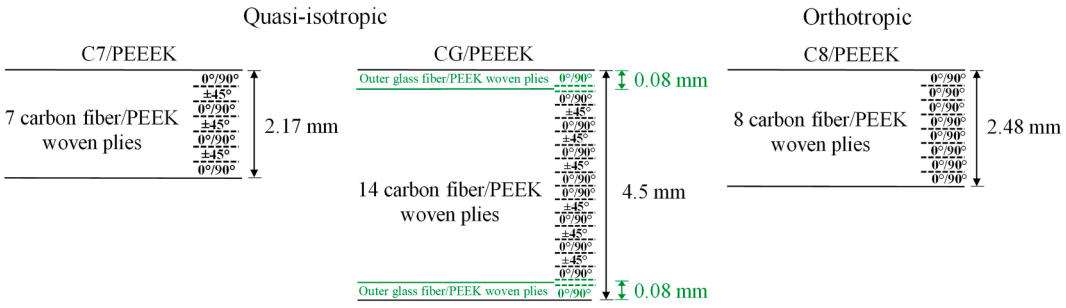

Fig. 2. Lay-up and thickness of the woven-ply composite laminates studied.

Table 2
A few properties of the elementary ply of woven carbon and glass fibers reinforced PEEK at RT and 150 °C.

	Carbon/PEEK		Glass/PEEK	
Nominal ply thickness (mm)	0.31		0.08	
T_g (°C)	143		143	
	TA	150 °C	TA	150 °C
Longitudinal modulus E_x (GPa)	60	55.04	22	
Transverse modulus E_y (GPa)	60	55.04	20	
Shear modulus G_{xy} (GPa)	4.83	4.43	6.55	
Poisson's coefficient ν_{xy}	0.04	0.037	0.04	

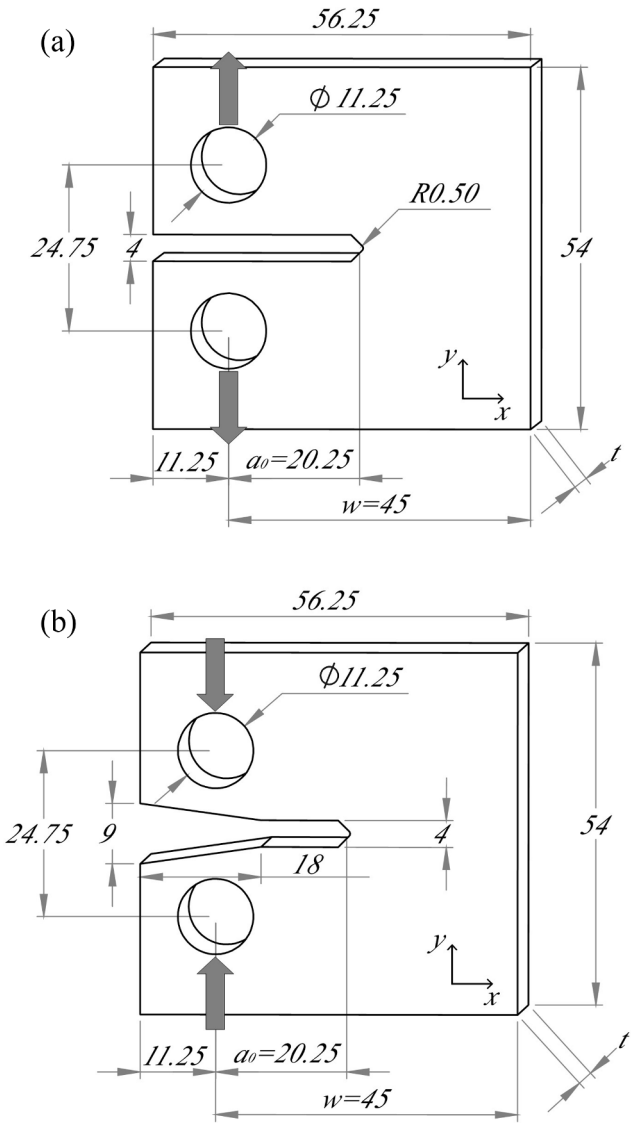

Fig. 3. Test specimen dimensions (in mm) for: (a) tension and (b) compression translaminar fiber-breaking fracture toughness tests.

$$\forall \boldsymbol{\varepsilon}_{xy}(\boldsymbol{x},\boldsymbol{y}) \neq 0 \Rightarrow \mathbf{F}_{\mathbf{T}}(\boldsymbol{x},\boldsymbol{y}) = 0$$

$$\forall \boldsymbol{\varepsilon}_{xy}(\boldsymbol{x},\boldsymbol{y}) = 0 \Rightarrow \mathbf{F}_{\mathbf{T}}(\boldsymbol{x},\boldsymbol{y}) = 1$$

$$\mathbf{F}_{\mathbf{T}}(\boldsymbol{x},\boldsymbol{y}) = -1$$

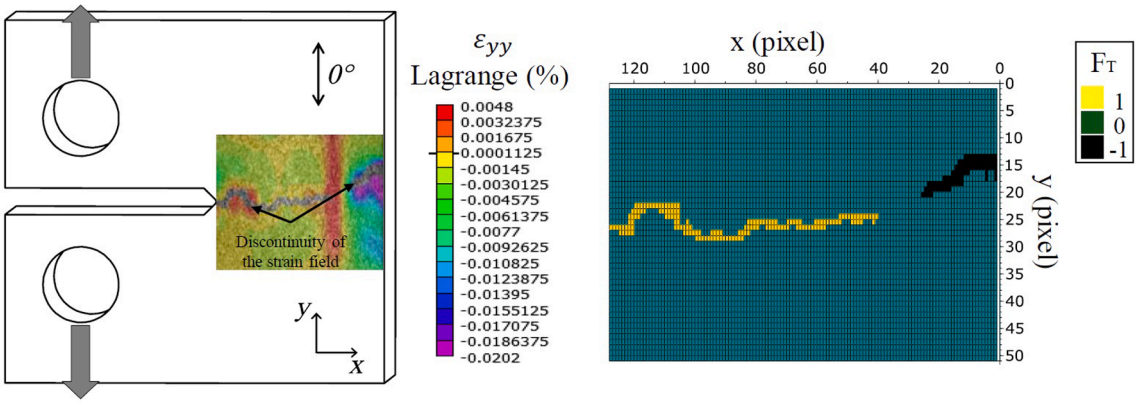

Fig. 4. FT function implemented on a CT specimen.

- $F_T = 0$ corresponds to the region for the undamaged area.
- $F_T = 1$ is the damaged area where a material discontinuity is present next to the initial crack tip and not information is computed using DIC.
- $F_T = -1$ is the damaged area where material discontinuity appears due to a secondary crack and not information is computed using DIC.

The crack length is then determined from the crack tip position in each pattern, independently of the orientation of crack within the pattern. The spatial resolution of the crack length is defined by the size of the subsets used in the DIC method.

3.3. Data reduction methods

3.3.1. ASTM-399 test standard

According to ASTM-399 test standard [32], initially developed and validated for metallic isotropic materials, the critical stress intensity factor (fracture toughness) in mode I (opening) K_{Ic} is given by:

$$K_{Ic} = \frac{P_c}{t\sqrt{w}} f(a/w) \tag{1}$$

with:

$$f(a/w) = \frac{2 + a/w}{(1 - a/w)^{3/2}} \left[0.886 + 4.64\left(\frac{a}{w}\right) - 13.32\left(\frac{a}{w}\right)^2 + 14.72\left(\frac{a}{w}\right)^3 - 5.6(a/w)^4\right]$$

where P_c is the critical load ensured at crack initiation, t is the thickness of the specimen, w is the distance from the load line to the right edge of the specimen (Fig. 3), a is the crack length, whose initial value is a_0 and $f(a/w)$ is a geometric correction function for a specimen of finite width [2,37]. Eq. (1) is only defined for isotropic materials though the studied laminates are not completely isotropic. To a fist approximation and for comparison purposes, the function f(a/w) proposed for isotropic materials has been used to compute the values from the method proposed in ASTM-399 test standard. It is acceptable for C7/PEEK and CG/PEEK laminates. For the C8/PEEK orthotropic materials, the solution proposed by Ortega et al for a CT specimen should be considered in order to obtain the linear elastic fracture toughness, *the* stress intensity factor and the compliance at the load line [36]. The solution applies for any orthotropic material whose principal directions are defined by the crack direction, assuming that the crack grows along the symmetry plane of the specimen.

The critical energy release rate of the laminate G_{Ic}^{lam} is then calculated from K_{Ic} [37–38]:

$$G_{Ic}^{lam} = C_I K_{Ic}^2 \tag{2}$$

where C_I is the orthotropic elastic coefficient in plane-stress conditions defined by [37]:

$$C_I = \sqrt{\frac{1}{2E_xE_y}} \sqrt{\sqrt{\frac{E_x}{E_y}} - \nu_{xy} + \frac{E_x}{2G_{xy}}}$$

where E_x, E_y, G_{xy} and ν_{xy} are respectively the Young's modulus in x and y directions (Fig. 1), the shear modulus and the Poisson's ratio of the laminate. The properties used for the computation of the orthotropic elastic coefficient of the equivalent laminate are given in Table 3, they are obtained from the properties of the elementary ply (Table 2) using the laminate theory. The influence of temperature

has been taken into account on the properties of the laminates from the standardized tensile tests carried out on different laminates [15,30].

3.4. Compliance method

The compliance method is commonly used to calculate the evolution of the energy release rate from the force-displacement curve at the initiation and propagation of the crack, making it possible to determine the evolution of compliance $\boldsymbol{C} = \boldsymbol{d}/\boldsymbol{P}$ (Fig. 5), where d is the displacement and P the force:

$$G_I^{lam} = \frac{P_c^2}{2t}\left(\frac{dC}{da}\right) \tag{3}$$

Classically a cubic function of the compliance function versus the crack length has been fitted on the whole test for each experiment [5–6], then an analytical derivation has been done to evaluate the fracture toughness.

4. Results and discussion

4.1. Thermo-mechanical behavior

In order to compare the thermo-mechanical responses of the studied laminates (whose thicknesses are different), the force was normalized by the thickness of the laminate.

4.1.1. Tensile tests

The propagation of the macroscopic crack is identified from the jumps observed on the force-displacement curves. The method defined in Section 3.2 then makes it possible to monitor the evolution of the crack length via the gradual decrease in load during propagation (Fig. 6). From the curves in Fig. 6, it is observed that quasi-isotropic laminates have similar macroscopic responses with a quasi-linear force-displacement curve before crack propagation, but with a higher initiation load at fracture for the CG/PEEK material. The significant non-linearity observed on the C8/PEEK curve is due to its low shear modulus and to a zone of high plasticity induced by significant damage at the initial crack tip (intrinsic toughness) (Fig. 7) as well as to localized crushing in the zones where the mechanical load imposed by the axes of the intermediate tool (extrinsic toughness) [31,39–40]. It appears that the shear deformation field of the orthotropic lay-up (Fig. 7) extends beyond the crack tip, causing a more pronounced plastic behaviour. In addition, the larger plasticity zone at the loading axes may justify a slower crack propagation in comparison to quasi-isotropic laminates due to a higher dissipated mechanical load.

Overall, the influence of temperature is not significant, despite the increase in the ductility of the resin at 150 °C. The influence of temperature is also analyzed by examining the post-mortem damage. Macroscopic observations of the damaged area suggest that the ruin of the quasi-isotropic laminates occurs by translaminar failure of the fibers in tension at TA. At 150 °C, the onset of compressive failure in the area opposite the initial notch was observed for the CG/PEEK laminate (Figs. 6 and 8b). This compressive fracture is associated with buckling on a macroscopic scale, which can be explained by the significant increase in ductility of the PEEK matrix at $T > T_g$ by degrading its shear strength in particular. The C8/PEEK orthotropic laminates exhibit an elastic-ductile behaviour (Fig. 6c). The influence of temperature remains moderate (about 20% on the fracture load of the first fiber bundle), but results in a very pronounced out-of-plane displacement requiring the use of an anti-buckling device. The orthotropic stacking sequence fosters a very gradual propagation of the crack, with jumps of less than 1 mm (Fig. 6c).

4.1.2. Compressive tests

In CC specimens, crack growth is mainly related to micro-buckling of the plies at 0°, which results in fiber breakage in compression and the formation of a kink-band. Using the same protocol as for the CT specimens, the crack tip in the area damaged by compression fiber breakage could be located by image analysis. It can be seen that the crack growth is gradual (Fig. 9), but the correspondence between the increases in crack length and the jumps observed on the force-displacement curve is not obvious. In addition, it appears that the first fiber failure does not correspond to the maximum force, but that the load continues to increase for some time after this first failure. This is because the fiber breakage in compression is less abrupt than in tension, and that after the failure in compression a crushing stress continues to be transmitted.

From the curves in Fig. 9, it can be noted that quasi-isotropic laminates are characterized by similar macroscopic responses, the

Table 3
Elastic properties of the equivalent orthotropic laminate.

	C7/PEEK quasi-isotropic [(0/90),(±45),(0/90),(±45),(0/90),(±45),(0/90)]				CG/PEEK quasi-isotropic $[(0/90)_G,(0/90),(\pm45),(0/90),(\pm45),(0/90),(\pm45),(0/90)]_S$				C8/PEEK orthotropic $[(0/90)]_8$			
	E_x(GPa)	E_y(GPa)	G_{xy}(GPa)	ν_{xy}	E_x(GPa)	E_y(GPa)	G_{xy}(GPa)	ν_{xy}	E_x(GPa)	E_y(GPa)	G_{xy}(GPa)	ν_{xy}
TA	46.57	46.57	15.12	0.25	45.73	45.66	14.82	0.25	60	60	4.83	0.04
150 °C	42.73	42.73	13.91	0.25	42.03	41.96	13.65	0.25	55.04	55.04	4.43	0.04

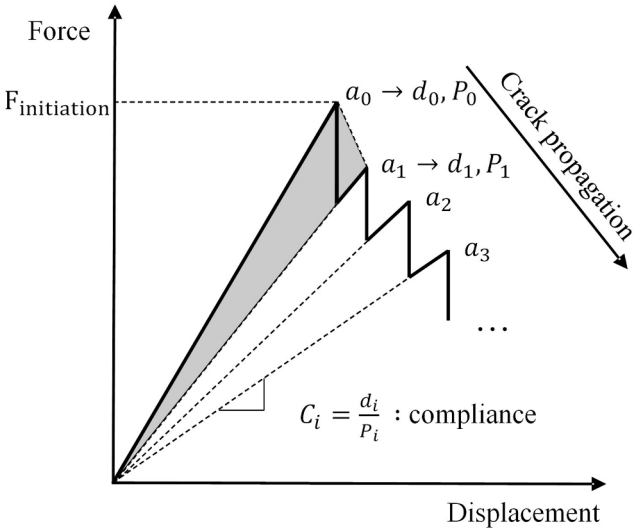

Fig. 5. Force-displacement curve representative of a stable crack propagation.

force-displacement curve is quasi-linear until the start of propagation, but unlike the case of the CT tests, the load continues to increase after the start of propagation up to about 5 mm crack length. It is also observed that the failure of the first fiber bundle occurs almost at the same time in the force-displacement curve for quasi-isotropic laminates. The glass plies, as well as the greater thickness of the CG/PEEK, therefore do not seem to significantly influence the resistance to fracture initiation, but delay the growth of the crack.

In compression, the influence of temperature is very pronounced with a decrease of about 35% in fracture initiation resistance for quasi-isotropic laminates. At room temperature, the specimens are characterized by a final quasi-brittle fracture, which results in a two-part separation of the specimens along the axis of the initial crack (Fig. 10a); this self-similar translaminar fracture [1] occurs when the crack length reaches a critical value due to the stress concentration accumulated on the free-edge of the specimen during the test. The onset of a tensile fiber breakage at the free-edge of the specimen is observed at 150 °C for quasi-isotropic laminates (Fig. 9a and b). At 150 °C, the more pronounced ductility of the PEEK matrix fosters the localized crushing of the plies in compression inducing ductile failure, especially for the orthotropic laminate.

The force-displacement curve of the C8/PEEK orthotropic laminate (Fig. 9c) is non-linear even before propagation begins. At room temperature, and at 150 °C, the orthotropic C8/PEEK laminate does not exhibit fiber breakage in tension; the fibers all fail in compression. This is explained by the absence of plies at ±45°, which limits the transmission of shear forces. At 150 °C, the test was interrupted before the final break to avoid contact between the notch faces of the specimen, but the specimen was not completely broken (the load does not decrease to 0). This interruption is likely to prevent the development of a tensile crack, observed in quasi-isotropic laminates. The influence of temperature is more pronounced compared to the quasi-isotropic laminates with a reduction of about 50% of the resistance at the initiation of the fracture.

4.2. Estimation of the strain energy release rate

The resistance of a laminate to translaminar crack initiation and propagation are characterized by a resistance curve, called the R-curve. The first point of the R-curve can be defined as the critical energy release rate related to crack initiation $\boldsymbol{G_I^C}$, while the propagation values $\boldsymbol{G_I^C}$ during propagation generally tend towards an asymptote [3,5–11,14,17–19]. Here, the ASTM-399 test standard is only applied to determine the value of the critical initiation energy release rate, the critical load associated with crack initiation was identified using digital image analysis. The compliance method is used to monitor the evolution of the energy release rate during propagation as well.

4.2.1. Tensile tests

The mean R-curves obtained for the three laminates are shown in Fig. 11. No value was taken for a crack length greater than 11 mm due to the appearance of a secondary crack (compression crack for the CT test and tensile crack for the DC test), which contributes to dissipation of mechanical energy during fracture, which disturbs the evaluation of the strain energy release rate.

The compliance method makes it possible to monitor the evolution of the energy release rate during crack propagation (Fig. 11). The values of $\mathbf{G_I^C}|_{\boldsymbol{tension}}$ at initiation determined from the ASTM-399 standard seem to validate its use for quasi-isotropic woven laminates; the difference observed at the values obtained with the compliance method remains small (Fig. 14). For the orthotropic C8/PEEK laminate, the mean value of $\mathbf{G_I^C}|_{\boldsymbol{tension}}$ at initiation calculated from ASTM-399 gives a value at RT of 29.9 kJ/m^2 compared to 117.3 kJ/m^2 for the compliance method. It is reasonable to assume that the higher value of $\mathbf{G_I^C}|_{\boldsymbol{tension}}$ at initiation is due to a very high plasticity at the points of load application accompanied by a greater area of plasticity at the crack tips (Fig. 7). It is worth noting that

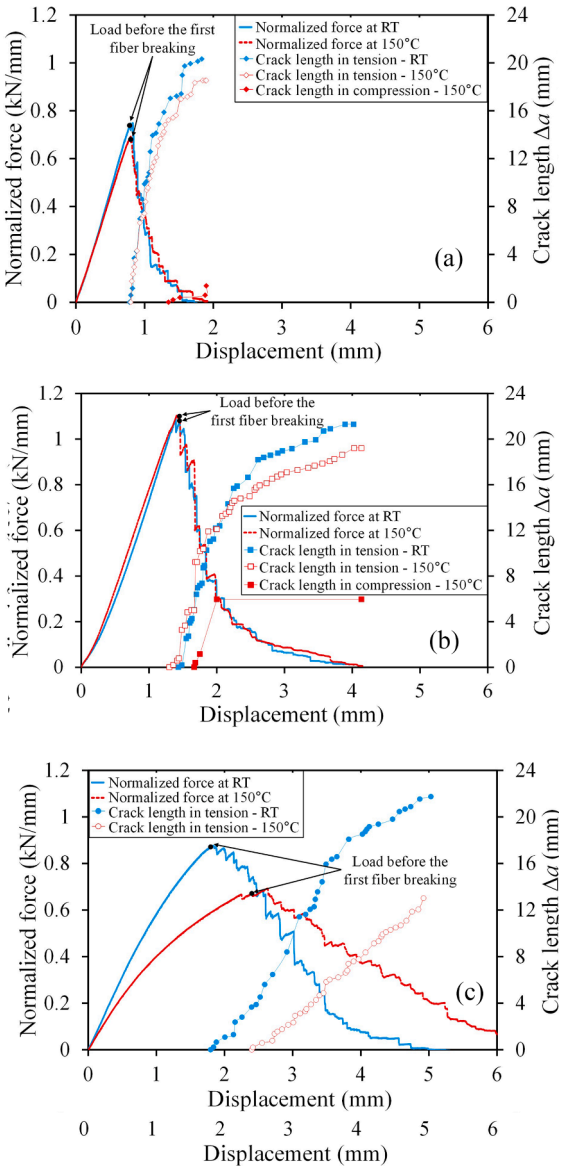

Fig. 6. Macroscopic mechanical responses and evolution of the crack length (based on the DIC analyze) of the different laminates in the case of CT specimens at RT and 150 °C.

ASTM-399 is applicable for materials with elastic-brittle behaviour, which is not observed for orthotropic laminates (Fig. 6-c).

Fig. 11 shows that all the R-curves tend to converge for a crack length greater than about 4–11 mm depending on the case, this would mean that the size of the FPZ is reached from the beginning and does not change much. For quasi-isotropic laminates, it is observed that the increase in thickness implies a significant increase in $\mathbf{G_I^C}|_{tension}$ at initiation and during propagation (Fig. 11 and Fig. 14). The presence of two glass-PEEK plies can be considered negligible compared to the proportion of carbon-PEEK plies in the CG/PEEK hybrid laminate [28], so the large increase observed can be attributed mainly to the increase in the thickness of the laminate [6,10–11,20], which leads to an increase in the size of the damaged areas (Fig. 12). A simple thresholding method applied in the images (Fig. 12) shows that the fracture surface increase with the thickness and with the presence of 45° laminate ply. Temperature contributes to a small increase (7–10%) in the translaminar fracture toughness of quasi-isotropic laminates at initiation; this trend is also observable during propagation (Figs. 11 and 14).

Overall, the C8/PEEK orthotropic laminate has a very high translaminar tensile fracture toughness compared to the quasi-isotropic laminates, while the number of fibers to be broken is lower (Fig. 12). In practice, cutting a 0°/90° ply requires cutting only the fibers at 0°, whereas cutting a ±45° ply requires cutting the fibers at +45° and −45° [10]. The greater toughness of the orthotropic laminate could be due to a zone of extensive plasticity caused by blunting at the initial crack tip (Fig. 7) as well as significant plastic deformations at the load application points, thus inducing energy dissipation, which is added to those due to the crack propagation.

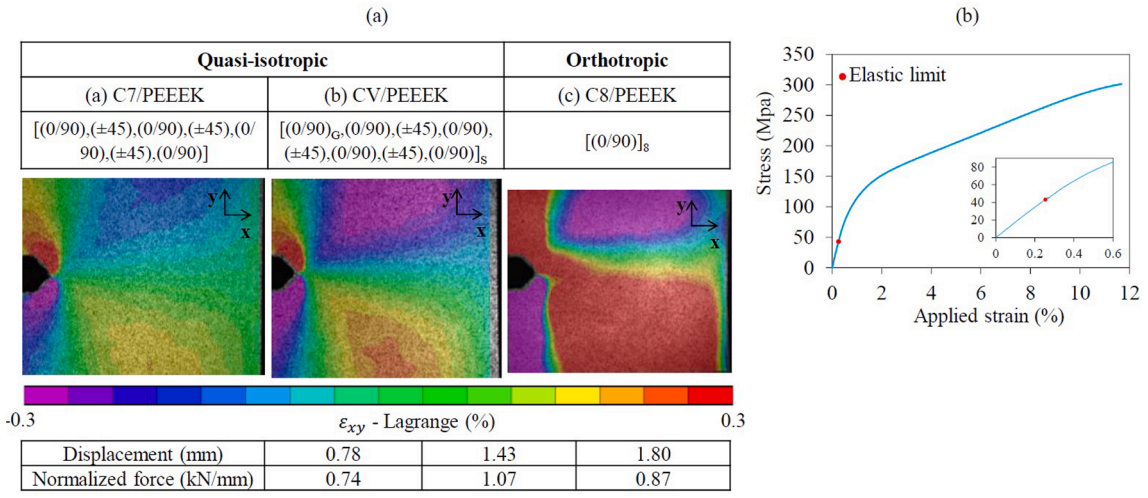

Fig. 7. (a) CT specimens at RT: shear deformation field at laminates' surface before failure of the first fibers bundles in the case – (b) Stress-Strain curve of angle-ply C8/PEEK laminates showing the onset of the plastic behavior at about 0.3% strain.

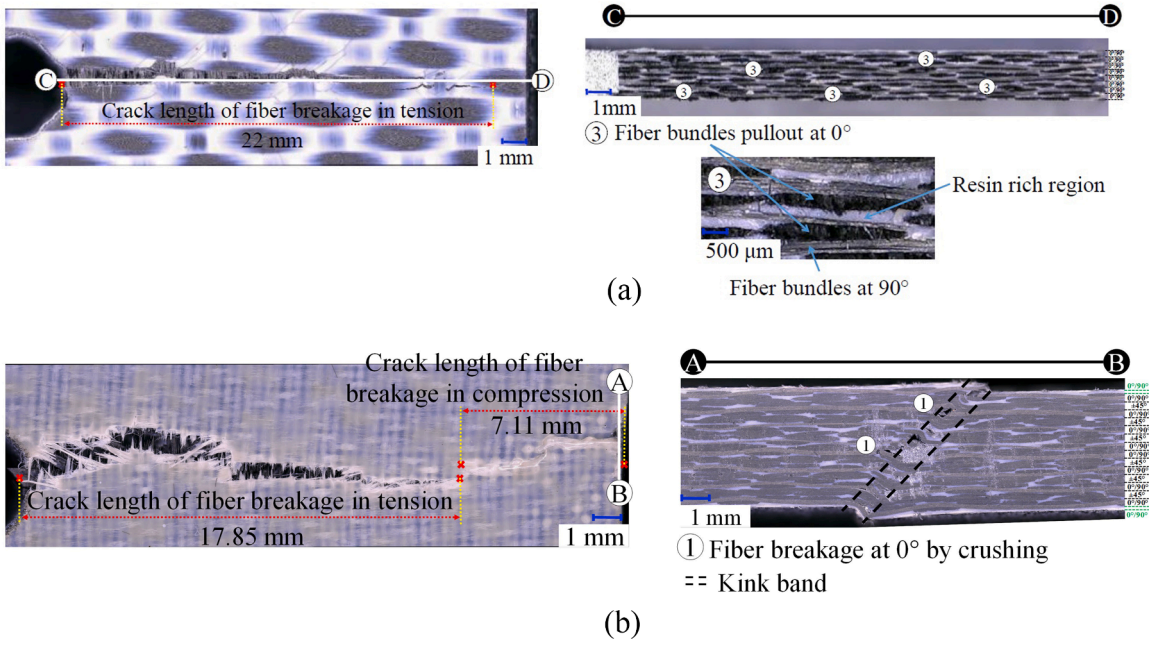

Fig. 8. Microscopic observations after failure of CT specimens: (a) C8/PEEK at RT - (b) CG/PEEK at 150 °C.

However, this calls into question the computation of the critical strain energy release rate from a global computation using the force-displacement curve (Fig. 11), and must be confirmed by a local computation of the integral J type or infrared thermography [18].

4.2.2. Compressive tests

In this case, R-curves were obtained for crack growth values up to about 16 mm (Fig. 13). An increasing trend of $\mathbf{G_I^C}|_{\mathbf{compression}}$ during propagation is observed for all laminates. This evolution is because after a compressive failure in the form of a kink-band, a crushing stress is transmitted (contrary to the case of a tensile test). Thus, the evolution of the critical energy release rate during the formation of a kink-band does not accurately describe the absorbed energy, since other modes of damage are present in particular the crushing of the fibers or the delamination. Thus, the values at initiation seem to be the best measure of the critical strain energy release rate associated with the appearance of the kink-band (Fig. 14). For quasi-isotropic laminates, an increase in translaminar fracture toughness can be observed with thickness, but not to the same magnitude as in tension. There is also a very marked decrease in translaminar fracture toughness on all the laminates studied at 150 °C (Figs. 13 and 14), in contrast to the tensile characterized by a

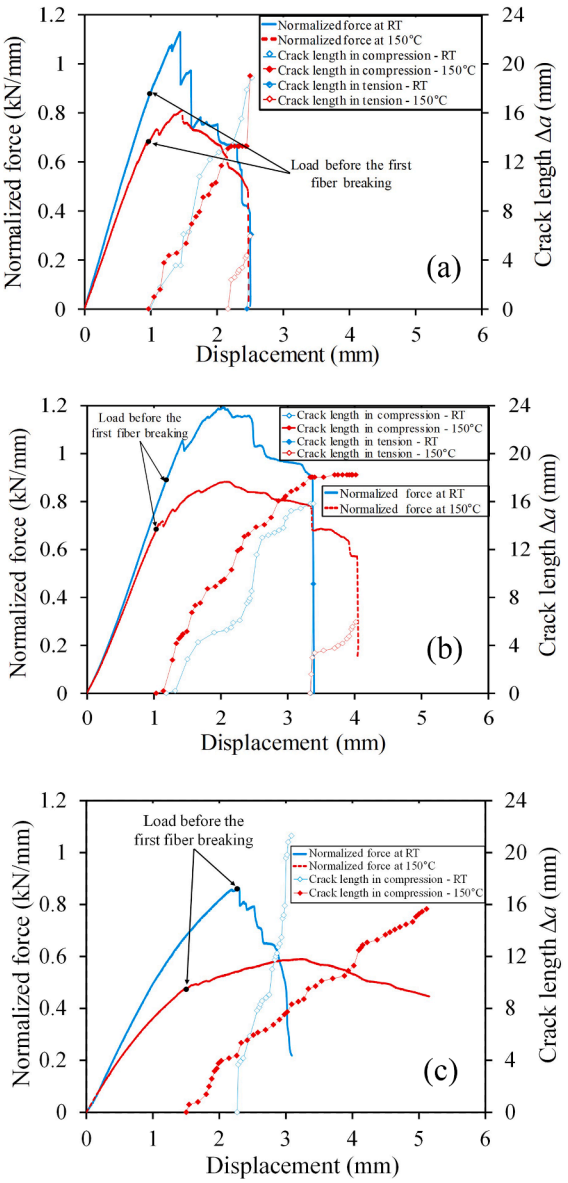

Fig. 9. Macroscopic mechanical responses and evolution of the crack length (based on the DIC analyze) of the different laminates in the case of CC specimens: (a) RT and (b) 150 °C.

slight increase, suggesting that a test temperature $T > T_g$ contributes to the formation of plastic buckling bands in compression due to increased ductility of the PEEK matrix. At RT the crushing is more pronounced than the buckling and at 150 °C the out-of-plane buckling is more pronounced than the crushing, because the softening of the matrix in the overlapping areas facilitates the out-of-plane displacement of the fiber bundles.

5. Conclusions

In order to study the damage tolerance of the high performance TP laminates used for aeronautical applications in high temperature conditions, the quantification of translaminar fracture toughness plays a key role. One of the main objectives of this study was to determine translaminar fracture toughness values for composite woven-ply thermoplastic-based laminates to be used under high temperature conditions. To authors best knowledge there are few references dealing with the translaminar fracture behavior and the quantification of fracture toughness of high-performance thermoplastic composites. In addition, an accurate measurement of the crack physical length during loading is challenging at room temperature, and even more at high temperature. This study was aimed at proposing an in situ crack growth measurement based on a Digital Image Correlation (DIC) technique implemented in a thermal chamber combined with a high intensity light source and a binarization algorithm.

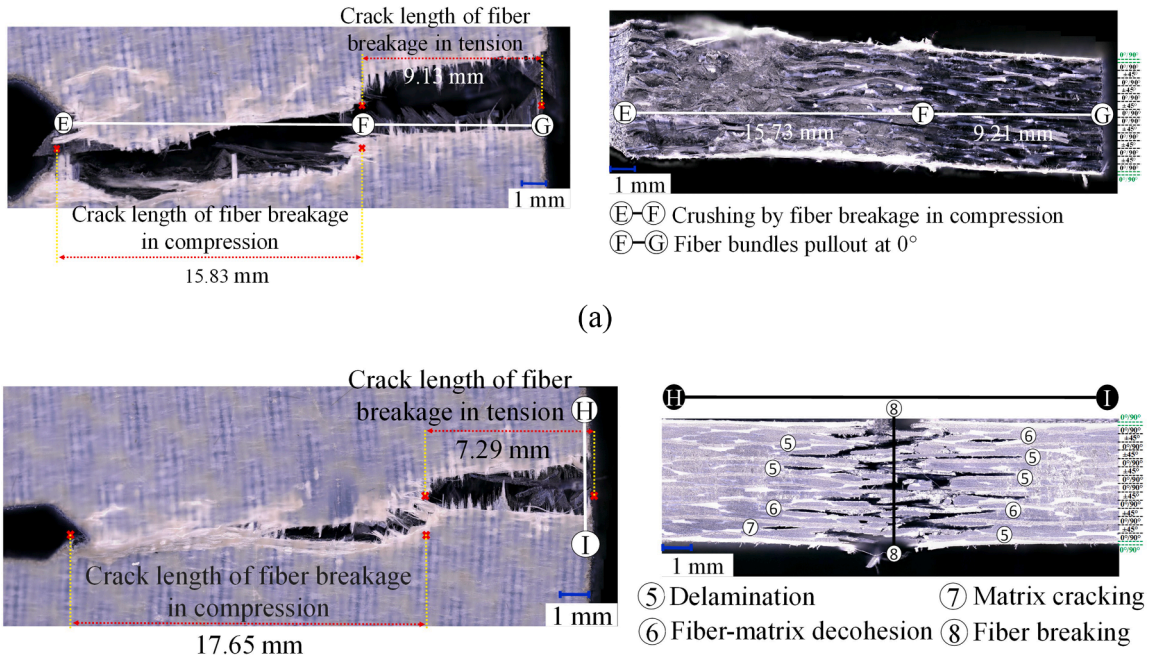

Fig. 10. Microscopic observations after failure of CG/PEEK CC specimens: (a) RT - (b) 150 °C.

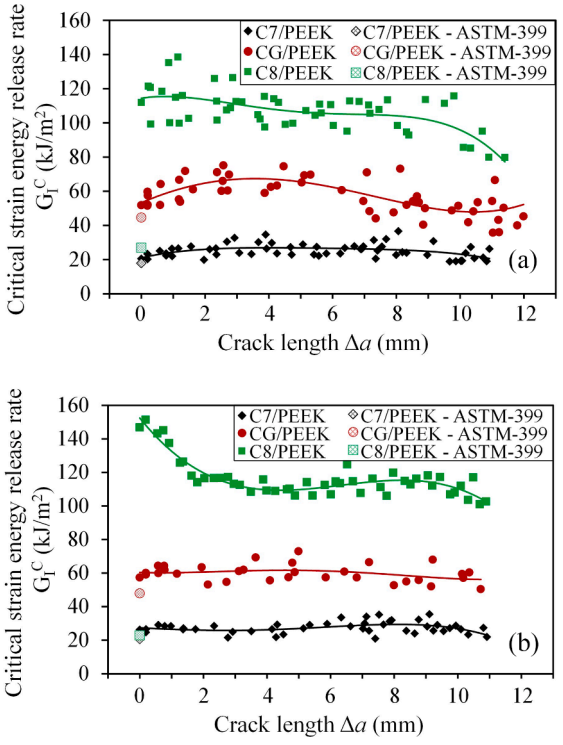

Fig. 11. R-curves obtained with the compliance method from CT specimen tests: (a) RT and (b) 150 °C.

In this study, Compact Tension and Compact Compression specimens were used to study the translaminar fracture on three thermoplastic laminates reinforced with woven-ply carbon fiber. Tests at room temperature and at 150 °C were carried out to study the effects of temperature when the ductility of the PEEK matrix is exacerbated.

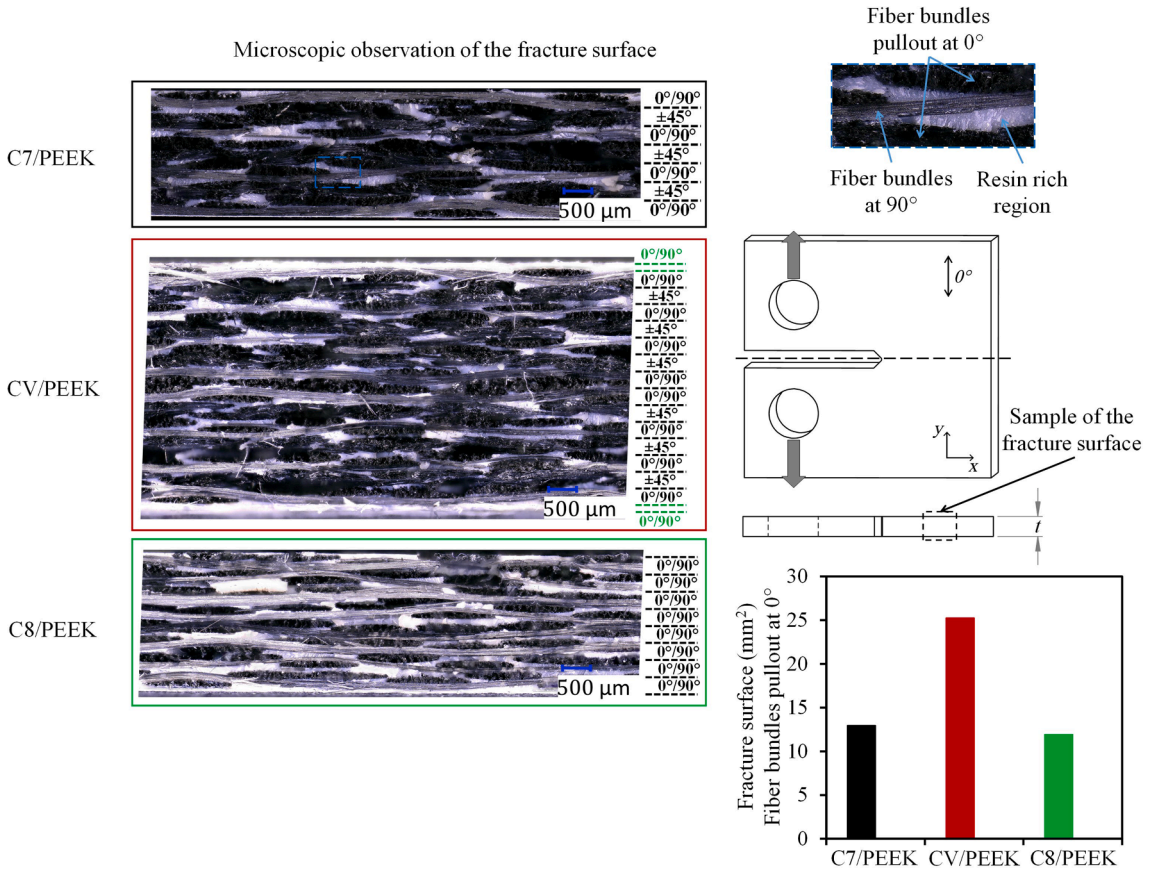

Fig. 12. Microscopic observations of the fracture surface of studied laminates in the case of CT specimens.

In orthotropic laminates, tensile tests also reveal that the plastic area is very large at the crack tip due to its low shear modulus (intrinsic toughness). Local plasticity also causes an important toughness linked to localized crushing in the area of force application (extrinsic toughness). In quasi-isotropic laminates, thickness contributes to increase the initiation load at fracture and slows the propagation of the crack. Compressive failure by plastic buckling on the edge opposite the notch is facilitated by the ductility of the PEEK matrix at $T > T_g$.

Compression tests show that compressive failure is driven by the fiber breakage at 0° and the formation of a plastic kink-band. As for tension tests, for the orthotropic laminate, the low shear modulus induces an important zone of plasticity, an important extrinsic toughness and makes it difficult the evaluation of the fracture toughness. At high temperature, ductile failure associated with localized crushing of the plies is promoted by the plastic deformation of the PEEK matrix at $T > T_g$.

Toughness evaluation based on ASTM-399 proved to be relevant for quasi-isotropic woven laminates giving similar values compared to the compliance method. For highly orthotropic laminates, the computation of toughness based on an overall behaviour (force-displacement curve) is related to energy dissipation at the points of load application accompanied by greater plasticity mechanisms at the crack tip, which are combined with those related to crack propagation. In tension, the R-curves tend to converge towards an asymptote with an almost constant value, while in compression the R-curves tend to increase due to localized crushing which results in constant crushing stress.

Finally, at a temperature (e.g. 150 °C) slightly higher than the glass transition temperature of the materials there is a moderate increase in the translaminar fracture toughness in tension. Thickness increases the fiber pull out length causing an increase in the translaminar fracture toughness in tension. In compression, the thickness does not seem to influence the size of the kink-band (which is associated with the fiber diameter and to the matrix shear mechanical behavior). The compressive translaminar fracture toughness decreases sharply with the temperature, as the softening of the matrix in the overlapping areas facilitates the out-of-plane movement of the fiber bundles. For orthotropic laminates, the computation of the translaminar fracture toughness will have to be confirmed by a local computation of the J-integral type or infrared thermography due to the ductile fracture behaviour.

Declaration of Competing Interest

The authors declare that they have no known competing financial interests or personal relationships that could have appeared to influence the work reported in this paper.

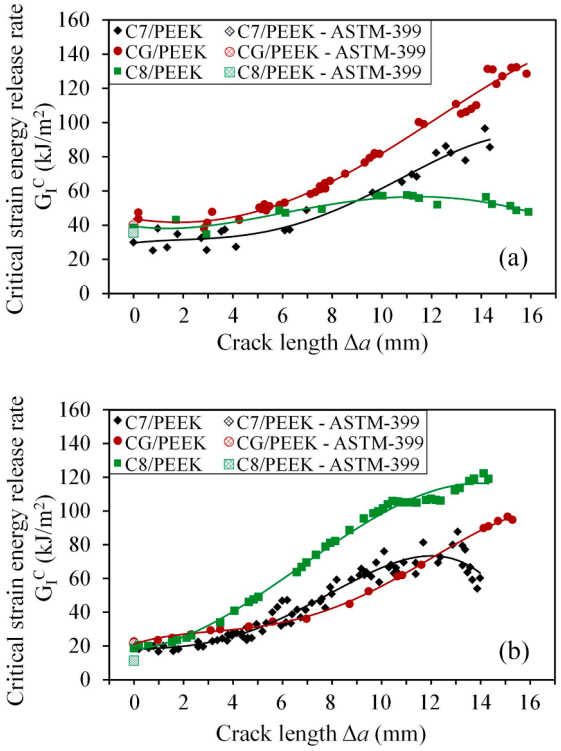

Fig. 13. R-curves obtained with the compliance method from CC specimen tests: (a) RT and (b) 150 °C.

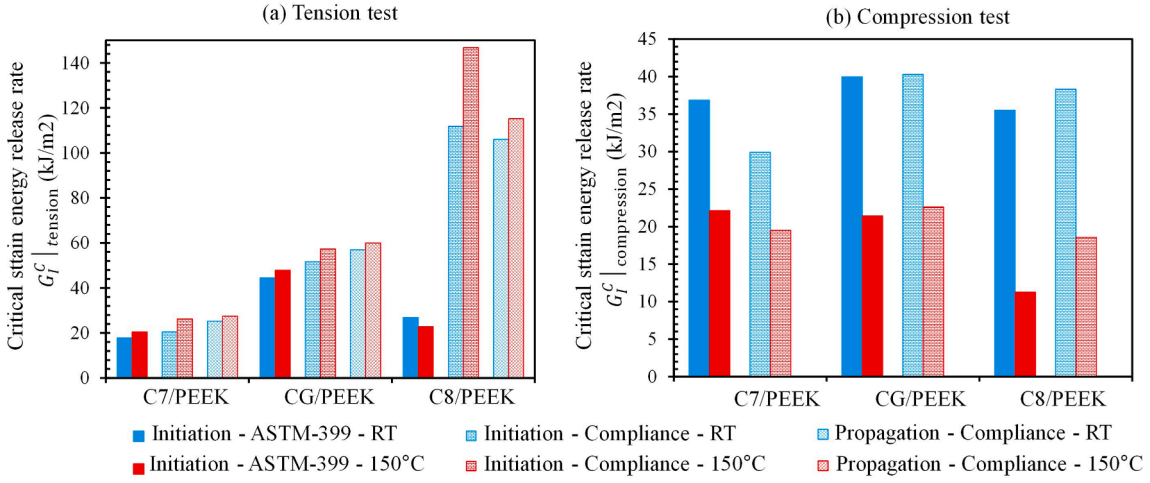

Fig. 14. Influence of the stacking sequence and the temperature on the tensile and compressive fracture toughness.

Acknowledgement

The authors would like to thank the Ministerio de Educación Superior, Ciencia y Tecnología (MESCYT) of the Dominican Republic for the funds invested in this research.

References

[1] Jones RM, Bert CW. Mechanics of composite materials; 1975.
[2] TAN S.C. – Stress concentration in laminated composites. Lancaster, Pa.: Technomic Pub. Co.; 1994.
[3] Pinho ST, Robinson P, Iannucci L. Fracture toughness of the tensile and compressive fibre failure modes in laminated composites. Compos Sci Technol 2006;66 (13):2069–79.

[4] Ortega A, Maimí P, González EV, de Aja JS, de la Escalera FM, Cruz P. Translaminar fracture toughness of interply hybrid laminates under tensile and compressive loads. Compos Sci Technol 2017;143:1–12.
[5] Laffan MJ, Pinho ST, Robinson P, Iannucci L. – Measurement of the in situ ply fracture toughness associated with mode I fibre tensile failure in FRP. Part I: data reduction. Compos Sci Technol 2010;70:606–13.
[6] Laffan MJ, Pinho ST, Robinson P, Iannucci L. – Measurement of the in situ ply fracture toughness associated with mode I fibre tensile failure in FRP. Part II: size and lay-up effects. Compos Sci Technol 2010;70:614–21.
[7] Mahmoud MK. Fracture toughness of single-edge notched fiber reinforced composite. Polym-Plast Technol Eng 2003;42(4):659–76.
[8] Catalanotti G, Camanho PP, Xavier J, Dávila CG, Marques AT. Measurement of resistance curves in the longitudinal failure of composites using digital image correlation. Compos Sci Technol 2010;70(13):1986–93.
[9] Laffan MJ, Pinho ST, Robinson P, Iannucci L, McMillan AJ. Measurement of the fracture toughness associated with the longitudinal fibre compressive failure mode of laminated composites. Compos A Appl Sci Manuf 2012;43(11):1930–8.
[10] Teixeira RDF, Pinho ST, Robinson P. Translaminar fracture toughness of CFRP: from the toughness of individual plies to the toughness of the laminate (Doctoral dissertation, Imperial College London); 2014.
[11] Teixeira RF, Pinho ST, Robinson P. Thickness-dependence of the translaminar fracture toughness: experimental study using thin-ply composites. Compos A Appl Sci Manuf 2016;90:33–44.
[12] Allaer K, De Baere I, Van Paepegem W, Degrieck J. Direct fracture toughness determination of a ductile epoxy polymer from digital image correlation measurements on a single edge notched bending sample. Polym Test 2015;42:199–207.
[13] Moore DR, Seferis JC. Intrinsic characterization of continuous fibre reinforced thermoplastic composites-I: toughness characterization of carbon fibre/polyether ether ketone (CF/PEEK) laminates. Pure Appl Chem 1991;63(11):1609–25.
[14] Slepetz JM, Carlson L. Fracture of composite compact tension specimens. In: Fracture Mechanics of Composites. ASTM International; 1975.
[15] Vieille B, Gonzalez JD, Bouvet C. Fracture mechanics of hybrid composites with ductile matrix and brittle fibers: Influence of temperature and constraint effect. J Compos Mater 2018; 0021998318802613.
[16] Wang TWH, Blum FD, Dharani LR. Effect of interfacial mobility on flexural strength and fracture toughness of glass/epoxy laminates. J Mater Sci 1999;34(19):4873–82.
[17] Rokbi M, Osmani H, Benseddiq N, Imad A. On experimental investigation of failure process of woven-fabric composites. Compos Sci Technol 2011;71(11):1375–84.
[18] Lisle T, Pastor ML, Bouvet C, Margueres P. Damage of woven composite under translaminar cracking tests using infrared thermography. Compos Struct 2017;161:275–86.
[19] Médeau V, Laurin F, Rannou J, Hurmane A, Quillent H, Lachaud F. Robust characterization of crack propagation in 3D woven composites and evidences of size dependency. Compos Struct 2019. 111175.
[20] Jose S, Kumar RR, Jana MK, Rao GV. Intralaminar fracture toughness of a cross-ply laminate and its constituent sub-laminates. Compos Sci Technol 2001;61(8):1115–22.
[21] Laffan MJ, Pinho ST, Robinson P, McMillan AJ. Translaminar fracture toughness testing of composites: A review. Polym Test 2012;31(3):481–9.
[22] Tretyakov MP, Wildemann VE. Stable crack growth in composite laminates under various stiffness of the loading system. Procedia Struct Integrity 2017;5:233–8.
[23] John R. Stress intensity factor and compliance solutions for an eccentrically loaded single edge cracked geometry. Eng Fract Mech 1997;58(1–2):87–96.
[24] Anderson TL, Anderson T. Fracture mechanics: fundamentals and applications. Boca Raton, Fla.: Taylor & Francis; 2005.
[25] Coronado P, Argüelles A, Viña J, Mollón V, Viña I. Influence of temperature on a carbon–fibre epoxy composite subjected to static and fatigue loading under mode-I delamination. Int J Solids Struct 2012;49(21):2934–40.
[26] Kim KY, Ye L, Phoa KM. Interlaminar fracture toughness of CF/PEI and GF/PEI composites at elevated temperatures. Appl Compos Mater 2004;11(3):173–90.
[27] Yurchenko ME, Huang J, Robisson A, McKinley GH, Hammond PT. Synthesis, mechanical properties and chemical/solvent resistance of crosslinked poly (aryl-ether–ether–ketones) at high temperatures. Polymer 2010;51(9):1914–20.
[28] Vieille B, Chabchoub M, Bouscarrat D, Keller C. Prediction of the notched strength of woven-ply PolyPhenylene Sulfide thermoplastic composites at a constant high temperature by a physically-based model. Compos Struct 2016;153:529–37.
[29] Vieille B, Gonzalez JD, Bouvet C. Prediction of the ultimate strength of quasi-isotropic TP-based laminates structures from tensile and compressive fracture toughness at high temperature. Compos B Eng 2019;164:437–46.
[30] Vieille B, Aucher J, Taleb L. Comparative study on the behavior of woven-ply reinforced thermoplastic or thermosetting laminates under severe environmental conditions. Mater Des 2012;35:707–19.
[31] Launey ME, Ritchie RO. On the fracture toughness of advanced materials. Adv Mater 2009;21(20):2103–10.
[32] Standard, A. S. T. M. E399-12. Standard test method for linear-elastic plane-strain fracture toughness KIc of metallic materials. West Conshohocken, PA: American Society for Testing and Materials; 2012.
[33] Solutions Correlated. Vic 2D reference manual. Columbia: Correlated Solutions; 2009.
[34] Sutton MA, Mingqi C, Peters WH, Chao YJ, McNeill SR. Application of an optimized digital correlation method to planar deformation analysis. Image Vis Comput 1986;4(3):143–50.
[35] Scilab (Version 6.0.1). Available online: http://www.scilab.org/download/6.0.1.
[36] Ortega A, Maimí P, González EV, Ripoll Ll. Compact tension specimen for orthotropic materials. Compos A 2014;63:85–93.
[37] Tada H, Paris P, Irwin G. The analysis of cracks handbook. New York: ASME Press; 2000, 2, 1.
[38] Liebowitz H. Fracture: an advanced treatise. Volume VII. Fracture of nonmetals and composites; 1972.
[39] Liu H, Falzon BG, Catalanotti G, Tan W. An experimental method to determine the intralaminar fracture toughness of high-strength carbon-fibre reinforced composite aerostructures. Aeronaut J 2018;122(1255):1352–70.
[40] Blanco N, Trias D, Pinho ST, Robinson P. Intralaminar fracture toughness characterisation of woven composite laminates. Part I: Design and analysis of a compact tension (CT) specimen. Eng Fract Mech 2014;131:349–60.